

# Comparison of Reduced-FOV Single-Shot EPI Methods for DWI: ZOOM-EPI vs. 2D Echo-Planar RF Excitation

E. U. Saritas<sup>1</sup>, K-P. Hwang<sup>2</sup>, E. T. Han<sup>3</sup>, J. H. Lee<sup>1</sup>, D. G. Nishimura<sup>1</sup>, and A. Shankaranarayanan<sup>3</sup>

<sup>1</sup>Department of Electrical Engineering, Stanford University, Stanford, CA, United States, <sup>2</sup>Applied Science Laboratory, GE Healthcare, Houston, TX, United States, <sup>3</sup>Global Applied Science Laboratory, GE Healthcare, Menlo Park, CA, United States

**Introduction:** Single-shot EPI (ss-EPI) is widely used for diffusion-weighted imaging (DWI), due to its robustness against motion-induced phase perturbations. However, it is challenging to produce high-resolution DWI images with ss-EPI. Several reduced-FOV methods have recently been proposed to overcome this challenge [1-4]. In this work, we thoroughly compare two of these methods, ZOOM-EPI [1] and reduced-FOV with 2D echo-planar RF (2D-EPRF) excitation [2], by presenting sagittal and axial DWI of the spinal cord using both techniques.

**Methods:** Figure 1 shows the excitation schemes for the aforementioned reduced-FOV methods. The first method, ZOOM-EPI (Fig. 1.a), uses a 90° slice-selective pulse (a spectral-spatial RF pulse that also suppresses the signal from fat), followed by a 180° refocusing RF pulse applied obliquely at an angle  $\theta$ . The intersection of the resulting profiles is a parallelogram-shaped inner volume (light blue section in Fig. 1.a) that will be used for reduced-FOV imaging. This technique performs better if a slice skip is allowed between two adjacent slices, using an interleaved multiple-acquisition scheme (slice skip =  $N_{\text{acq}} \times \{\text{slice thickness} + \text{slice spacing}\}$ ). The parallelogram becomes more slanted for smaller slice skips, yielding an undesirably wide transition band (TB).

The second method (Fig. 1.b) uses a 90° 2D-EPRF excitation, with periodic sidelobes located  $\Delta d_{\text{replica}}$  distance apart in the slice-select (SS) direction. A refocusing 180° RF pulse is then applied to select only the main lobe of this excitation (light blue section in Fig. 1.b). The long duration of the 2D-EPRF pulse allows this excitation scheme to simultaneously suppress the fat signal (see [1] for details). Because the adjacent slices are not excited with this method, there is no need for a slice skip. However, the number of slices that can be imaged in a single TR is limited:  $\max(N_{\text{slices}}) = \Delta d_{\text{replica}} / \Delta d_{\text{ss}}$ , where  $\Delta d_{\text{ss}}$  is the slice thickness. To increase the number of slices, a longer RF pulse is needed, which increases the echo time (TE).

In this work, we incorporated these reduced-FOV methods into the same pulse sequence to ensure that the only difference is on the excitation side. *In vivo* cervical spine scans of healthy subjects were acquired on a 1.5T GE Excite scanner (40 mT/m gradients with 150 mT/m/ms slew rates) using an 8-channel CTL coil. For the sagittal comparison, 6 slices were acquired in a single acquisition (i.e., no slice skip). Meanwhile, two acquisitions were performed for the axial comparison, producing 24 slices for ZOOM-EPI and 16 slices for the 2D-EPRF method. We used a 62.5% partial k-space coverage, TR=3.6 s and  $\pm 62.5$  kHz bandwidth for the ss-EPI readout. Other imaging parameters are listed in Figures 2-3.

Multiple NEX images were combined with a refocusing reconstruction [5], where the central 12.5% of each single-shot data was used for phase correction. Partial k-space homodyne reconstruction [6] was then performed on the combined data.

**Results:** DWI images acquired with ZOOM-EPI and 2D-EPRF methods in the sagittal and axial planes are shown in Figures 2 and 3, respectively. Since a single acquisition is used in the sagittal plane, the parallelogram-shaped slice profile of ZOOM-EPI is quite slanted. This results in a signal dropout towards the edges in the PE direction. When multiple acquisitions are allowed as in the axial comparison, 2D-EPRF cannot image as many slices as ZOOM-EPI, due to the previously mentioned limit on the number of slices.

**Conclusion:** A thorough comparison is presented between two reduced-FOV methods, namely ZOOM-EPI and 2D-EPRF. 2D-EPRF is better suited when a single-acquisition is sufficient to cover the region of interest, as in sagittal imaging of the spine. In contrast, ZOOM-EPI performs better when many slices are needed, as in axial imaging of the spine. Therefore, these two sequences can be used complementarily, depending on the application's specific needs.

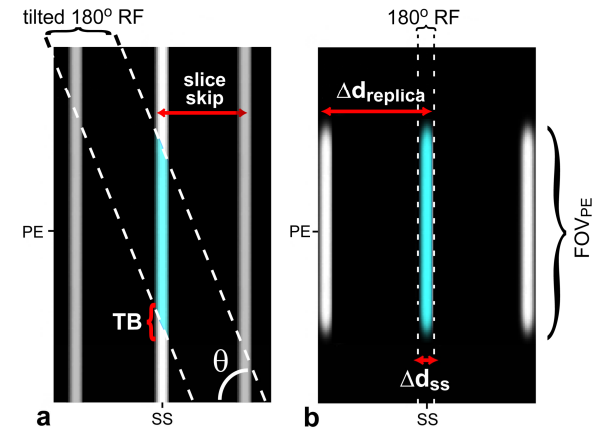


**Figure 1.** Excitation profiles: (a) ZOOM-EPI method, with regular 90° excitation and a tilted 180° RF pulse, creating a parallelogram-shaped inner volume. (b) The 2D-EPRF pulse and a 180° RF pulse that refocuses only the excitation in the main lobe. Light blue denotes the final profiles.

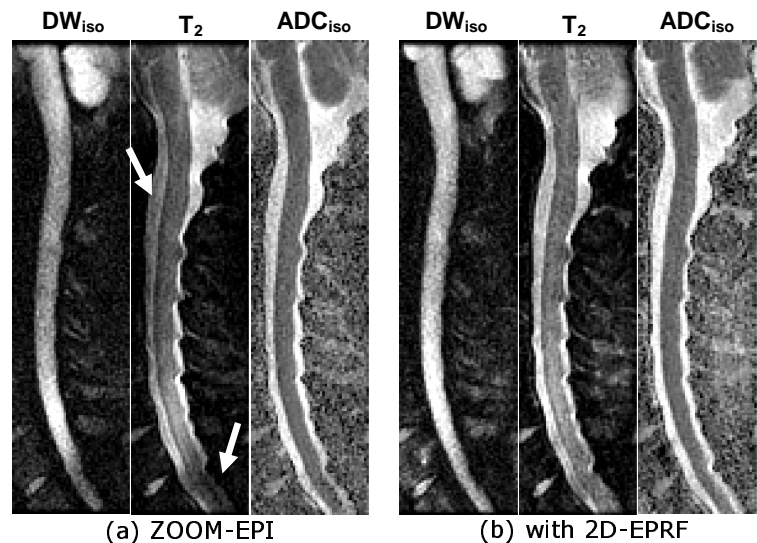


**Figure 2.** Sagittal comparison of (a) ZOOM-EPI and (b) 2D-EPRF. Note the shading in the ZOOM-EPI images (the white arrows) close to the edges in the PE direction, due to the parallelogram-shaped profile (Fig. 1.a). 6 slices are acquired for both techniques (only 1 shown), with 4 mm slice thickness, 0.4 mm slice spacing,  $0.94 \times 0.94 \text{ mm}^2$  in-plane resolution,  $18 \times 4.5 \text{ cm}^2$  FOV,  $b = 500 \text{ s/mm}^2$ ,  $TE = 64\text{ms}$ ,  $NEX = 10$ , total scan time = 2:24s.

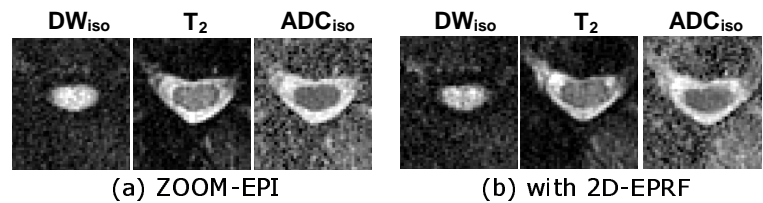


**Figure 3.** Axial comparison: (a) 24 slices with ZOOM-EPI and (b) 16 slices with 2D-EPRF are acquired in 2 acquisitions (only 1 slice shown). Note that the images with 2D-EPRF have slightly lower SNR due to a slightly longer TE (57 ms vs. 61 ms), and a narrower 180° RF profile. 5 mm slice thickness, 0.5mm slice spacing,  $0.83 \times 0.83 \text{ mm}^2$  in-plane resolution,  $8 \times 4 \text{ cm}^2$  FOV,  $b = 500 \text{ s/mm}^2$ ,  $NEX = 10$ , scan time = 4:48s.

**References:** 1. Wheeler-Kingshott, Neuroimage 16:93-102, 2002. 3. Jeong, MRM 54:1575-1579, 2005. 5. Miller, MRM 50:343-353, 2003. 2. Saritas, MRM 60:468-473, 2008. 4. Wilm, MRM 57:625-630, 2007. 6. Noll, IEEE TMI 10:154-163, 1991.